

**Binary wind capture &
accretion disk formation
numerical studies**

**BIPOLAR PREPLANETARY NEBULAE: HYDRODYNAMICS OF DUSTY WINDS IN BINARY SYSTEMS.
I. FORMATION OF ACCRETION DISKS**

NIKOS MASTRODEMOS AND MARK MORRIS

Model: 3D, SPH, dusty wind models, accretion disks formation about the binary companion to the mass-losing giant of asymmetric and bipolar PN.

Free parameters: wind velocity and binary separation.

Results: Permanent, stable, thin accretion disks form around the companion. Their equilibrium structure has elliptical streamlines with a range of eccentricities. Such disks may be susceptible to tilt or warping instabilities. Wind accretion in such binaries is stable, displaying no evidence for any type of flip-flop instability.

BIPOLAR PREPLANETARY NEBULAE: HYDRODYNAMICS OF DUSTY WINDS IN BINARY SYSTEMS. I. FORMATION OF ACCRETION DISKS

NIKOS MASTRODEMOS AND MARK MORRIS

Model: 3D, SPH, dusty wind models, accretion disks formation about the binary companion to the mass-losing giant of asymmetric and bipolar PN.

Free parameters: wind velocity and binary separation.

Results: Permanent, stable, the equilibrium structure has elliptical shape and can be susceptible to tilt or warp, but the models are displaying no evidence for any type of

PREPLANETARY NEBULAE

305

because of the high pressure buildup around the accreting companion, whereas an isothermal wind, $\gamma = 1$, will form a disk. In our early exploratory models with $\Gamma = \Lambda = 0$, we have confirmed that, without cooling, the temperature around a $1 M_{\odot}$ secondary exceeds 1.2×10^5 K and inhibits disk formation. In addition, Molteni, Belvedere, & Lanza-fame (1991) have shown that the shape and vertical extent of accretion disks from Roche lobe overflow in close binaries are sensitive to the value of the adiabatic index. They also find that a disk does not form for $\gamma \geq 1.2$. It is therefore evident that the particulars of the accretion process are determined by the efficiency of the cooling mechanisms.

BINARY MODEL INPUT PARAMETERS

Model	R_p (R_\odot)	T_{eff} (K)	L_p ($10^3 L_\odot$)	δ ($\times 10^{-3}$) ^a	d_b (R_p) ^b	n_s ^c
1	264.3	3000	5	6.5	3	550
2	264.3	3000	5	6.5	3	550
3	452.4	2400	6	5	4.5	650
4	452.4	2400	6	7.5	6	650

^a Dust to gas ratio by mass.

^b Binary separation in units of the primary's radius.

^c Number of SPH particles per boundary shell at the primary (see text).

TABLE 2

BINARY MODEL DERIVED PARAMETERS

Model	P (yr)	v_t (km s^{-1}) ^a	v_w (km s^{-1}) ^b	v_{acc} (km s^{-1}) ^c	R_{acc} (R_p) ^d	$r_{\text{acc}}/R_{\text{acc}}$ ^e	M_{acc} ^f	N
1	4.48	9	5	25	2.3	0.0043	13.2	62,000
2 ^g	4.48	9	5	25	2.3	0.0043	13.2	52,000
3	18.44	15	9	17.7	2.69	0.0024	12.4	59,000
4	28.38	25	17.3	21.8	1.77	0.0033	11.4	50,000

^a Terminal wind velocity for a single star.

^b Velocity the wind reaches at a distance equal to the binary separation (single star).

^c Wind velocity at the secondary in the corotating frame at the beginning of each run.

^d Hoyle-Lyttleton accretion radius in units of the primary's radius.

^e Ratio of accretion boundary to accretion radius.

^f Mach number in the corotating frame at the beginning of each run.

^g Parameters without considering the spin of the primary.

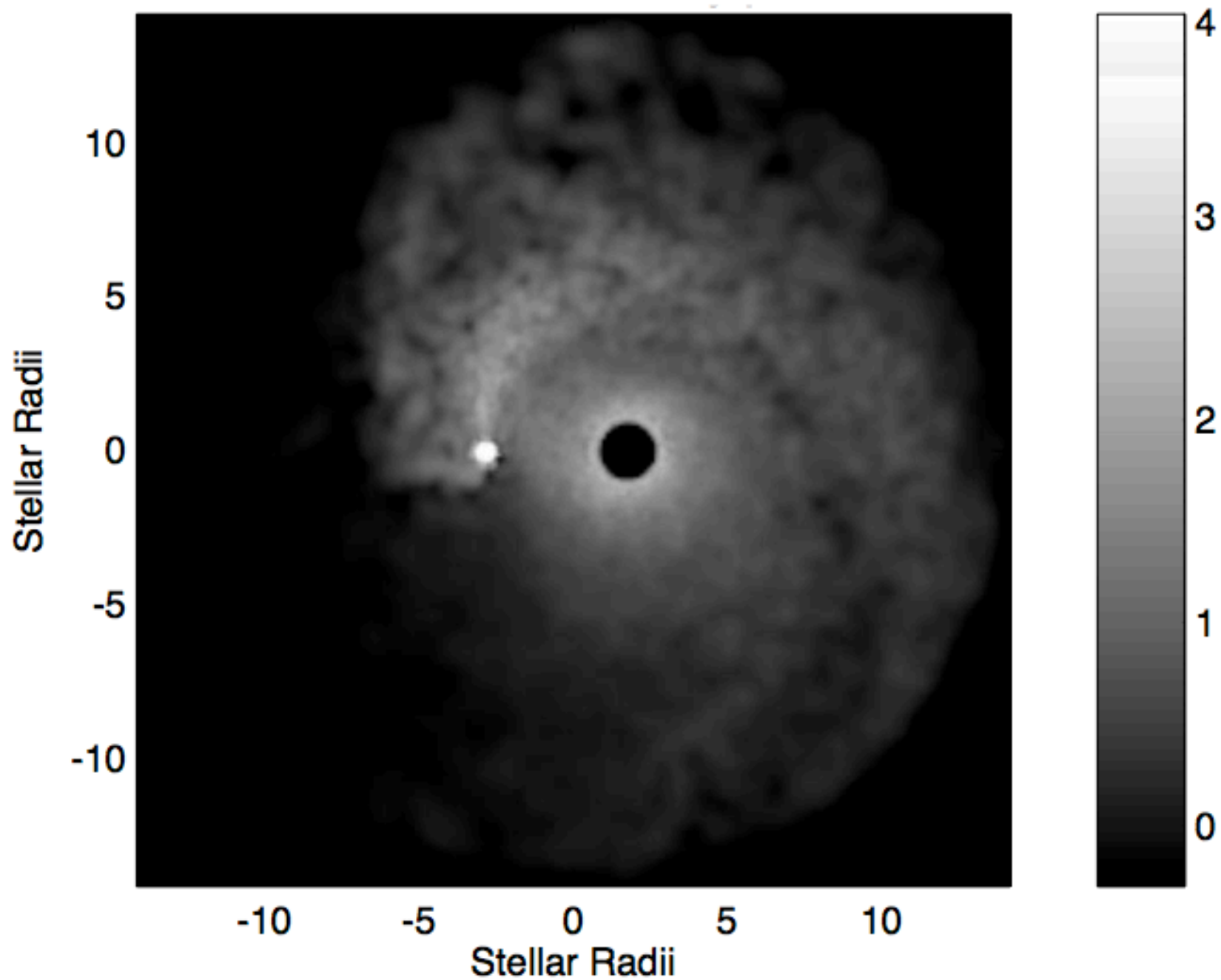
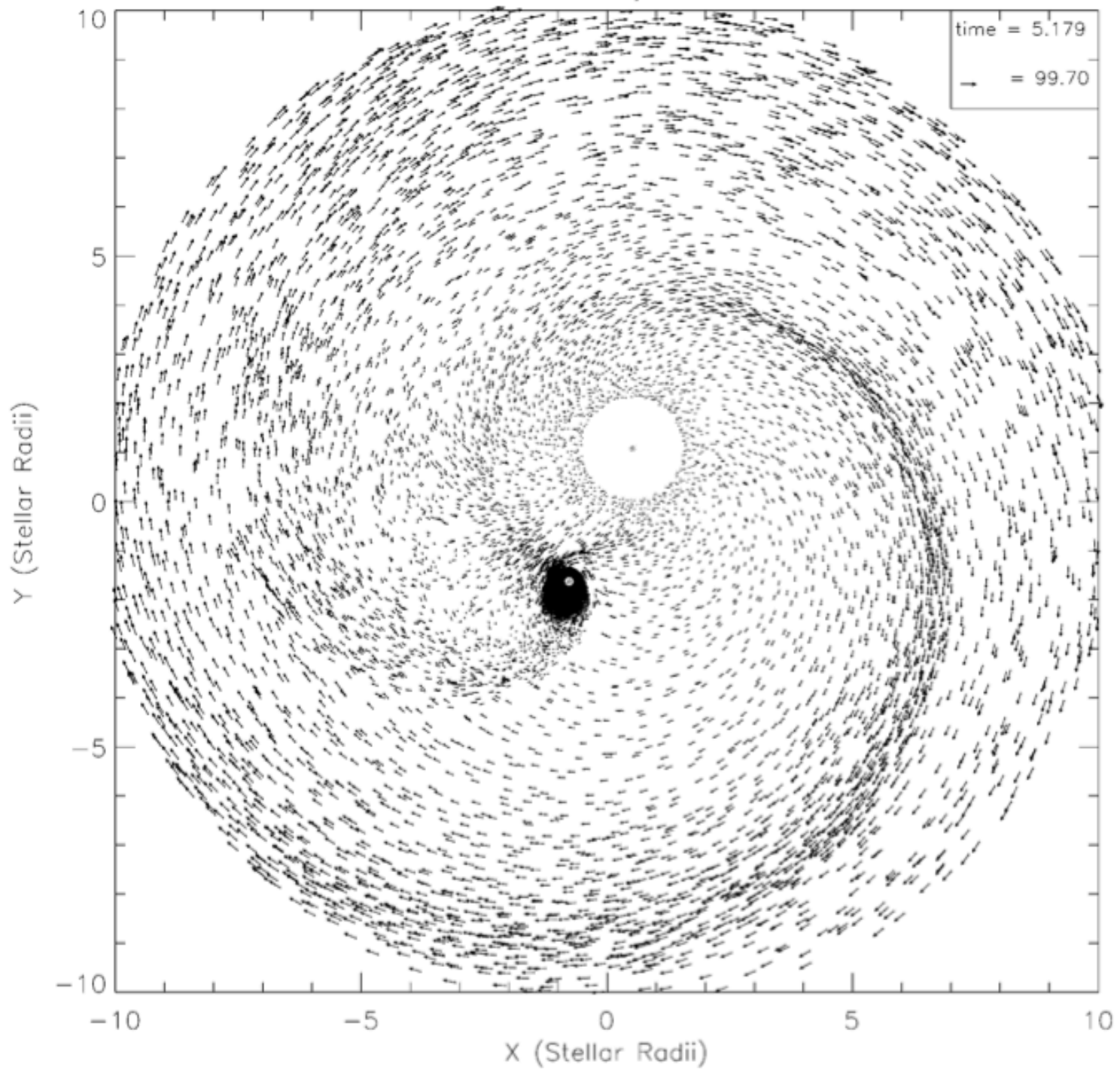
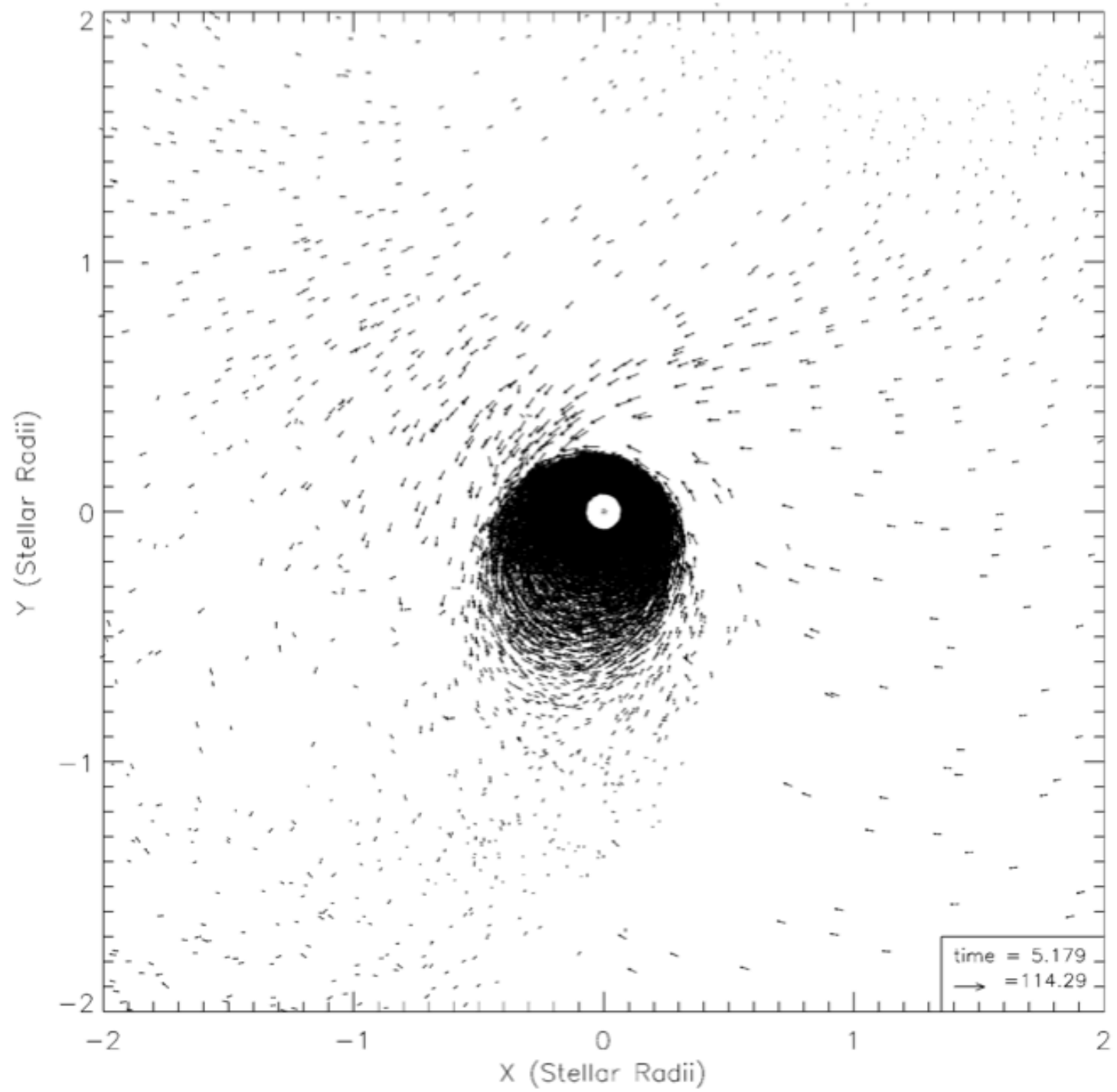


FIG. 6.—Gray-scale representation of the density on the equatorial plane for M3. The saturated black and white regions represent the interior of the mass-losing star, centered at $[1.8, 0]$, and the accretion disk around the secondary, centered at $[-2.7, 0]$, respectively. Density is shown on a logarithmic scale.





Disk radial density distribution

M1 ->

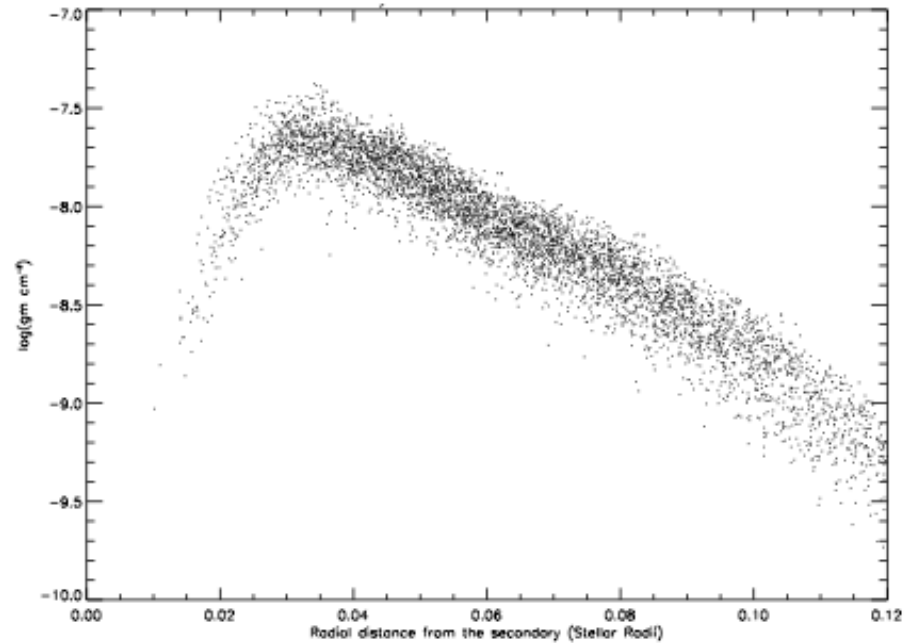


FIG. 15a

M2 ->

Same as M1 except
It has a spinning primary
Synchronized with
orbital motion

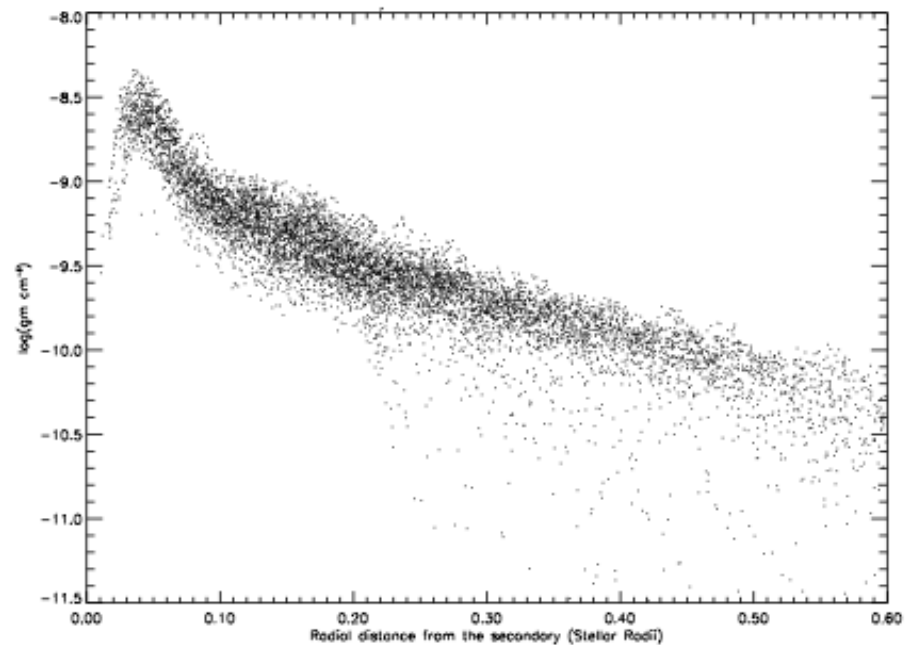


FIG. 15b

FIG. 15.—Radial density distribution of the accretion disks of (a) M1 and (b) M2. The origin of the horizontal axis is at the center of the accreting star, and the radial distance is in R_p . All particles within one smoothing length from the orbital plane are shown.

Two- and three-dimensional numerical simulations of accretion discs in a close binary system

Makoto Makita,^{★†} Kenji Miyawaki and Takuya Matsuda[★]

Model: 2D and 3D, accretion disc in a close binaries, flux vector splitting (SFS) finite volume method.

Free parameters: $\Upsilon = 1.01; 1.05, 1.1$ and 1.2 ,
 $M(\text{mass-losing star})/M(\text{mass-accreting star}) = 1$.

Results: Spiral shocks form on the accretion disc in all cases. The smaller g , the more tightly the spiral winds. $\text{Mach}_{\text{disk}} \leq 10$; lower than in observed accretion discs in close binaries.

2.4 Initial and boundary conditions

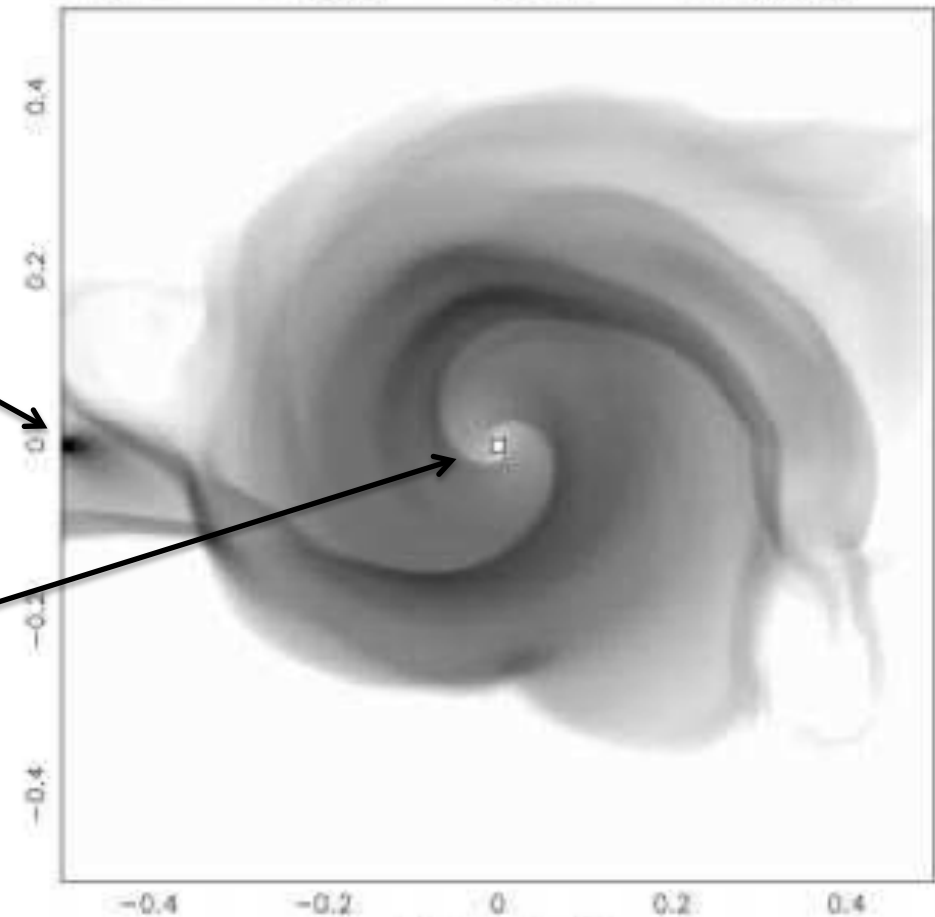
As an initial condition, we suppose that the whole computational region, which is $-0.5 \leq x, y \leq 0.5$ in 2D and furthermore $0 \leq z \leq 0.25$ in 3D, is filled with tenuous gas with a higher temperature at the initial instance. We assume $\rho_0 = 10^{-5}$, $p_0 = 10^{-4}/\gamma$ and $u_0 = v_0 = w_0 = 0$ in the whole numerical region.

This initial condition is also maintained outside of the outer boundary except for the L1 point and inside of the inner boundary during calculations. This choice forms the outer and the inner boundary conditions except for the inlet at the L1 point.

A small rectangular inlet hole is placed at the L1 point. The values at the inlet are $\rho_{\text{in}} = 1.0$, $p_{\text{in}} = 10^{-2}/\gamma$, $u_{\text{in}} = 0.01$ and $v_{\text{in}} = w_{\text{in}} = 0.0$ over the whole time period. This choice of the density and the pressure means that the sound speed of the gas to be injected into the computational region is 10^{-1} . Therefore, we may say that the temperature of the gas is very high. This is necessary to ensure a sufficient amount of gas flux from the inlet. The mass flux from the L1 point is computed by solving a Riemann problem, so the amount of inflow gas is not the same in the 2D and 3D simulations.

The **mass-accreting star** is represented by a hole of 3×3 cells in the 2D cases and $3 \times 3 \times 2$ cells in the 3D cases situated at the origin. We follow the time evolution until $t = 20\pi$ (that is 10

periods of revolution) in 2D calculations and $t = 10\pi$ in the 3D cases.



2D

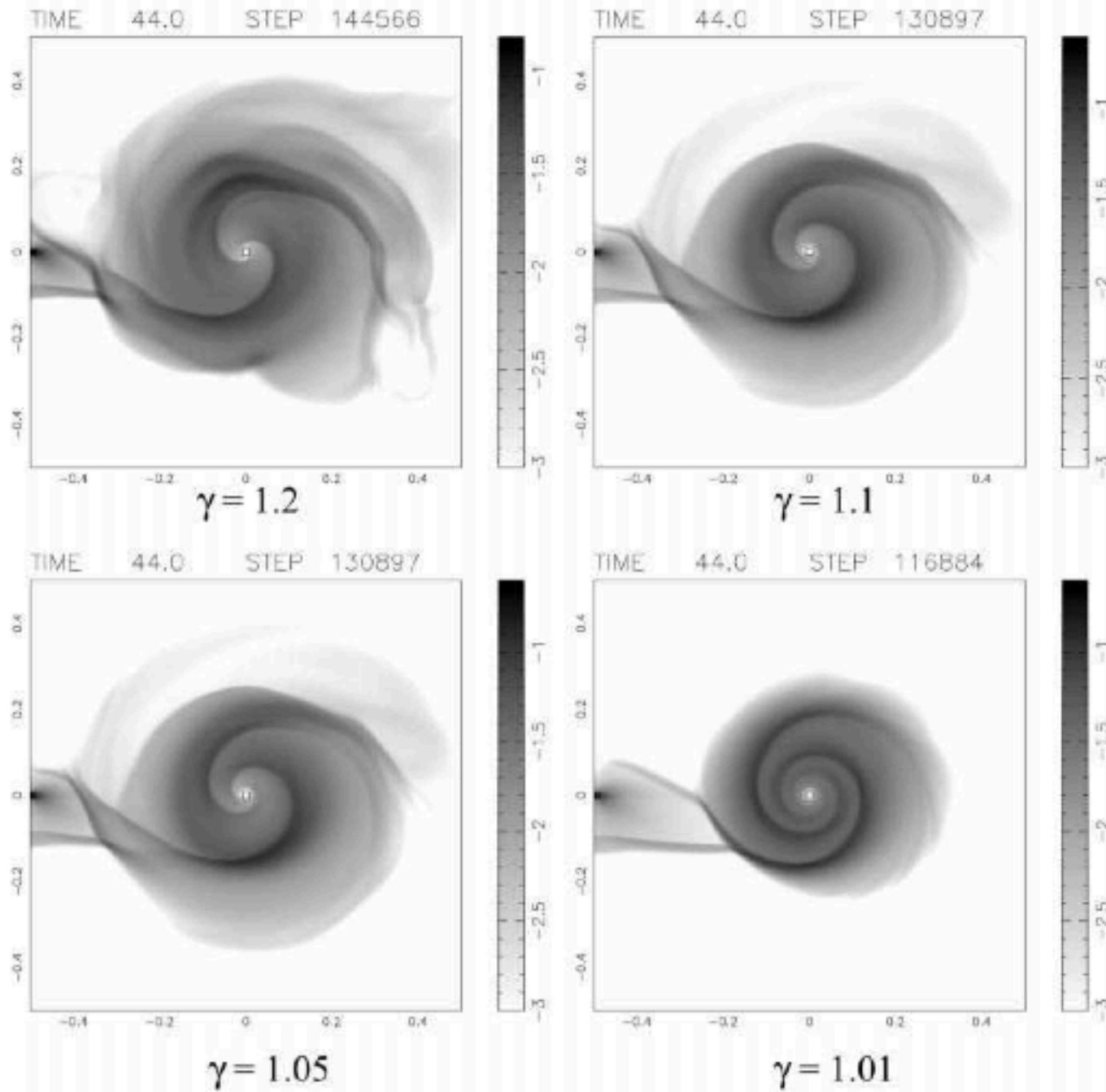


Figure 3. Grey-scale of the density distribution with a logarithmic scale after seven periods of revolution in the 2D calculations. The bar in the right-hand side shows the scale range.

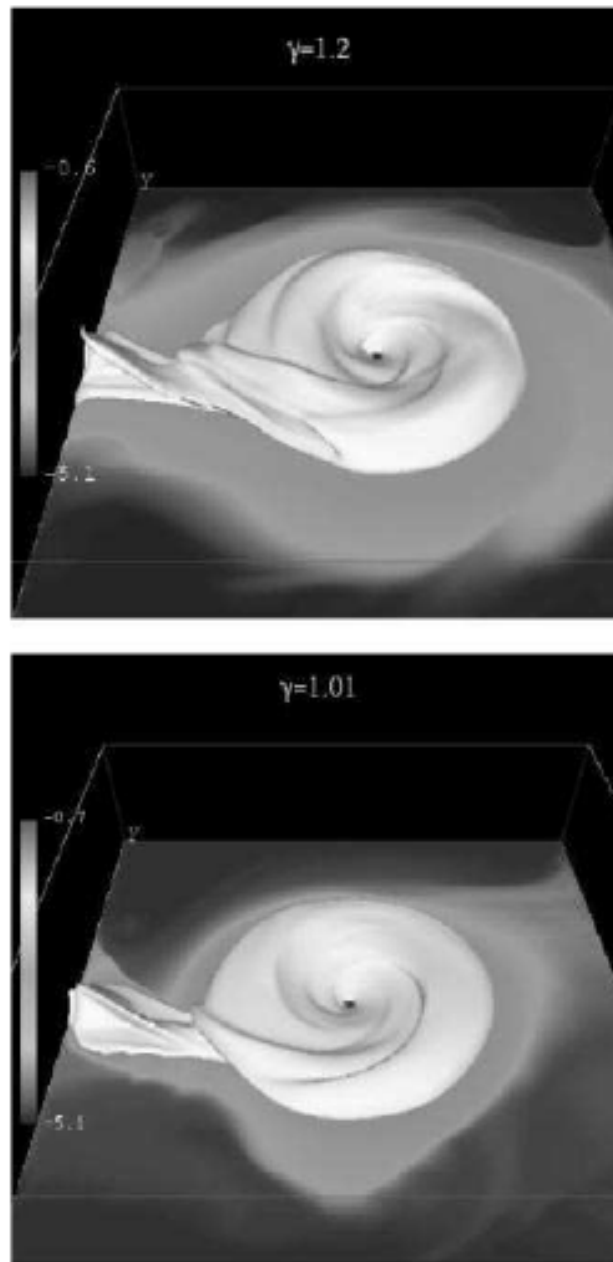


Figure 5. 3D view of the isodensity surface at the level of $\rho = -3$ with logarithmic scale after five periods of revolution. A grey-scale of the density in the orbital plane is also shown. The bar on the left-hand side shows the scale range.

Synthetic doppler maps (hodograph)

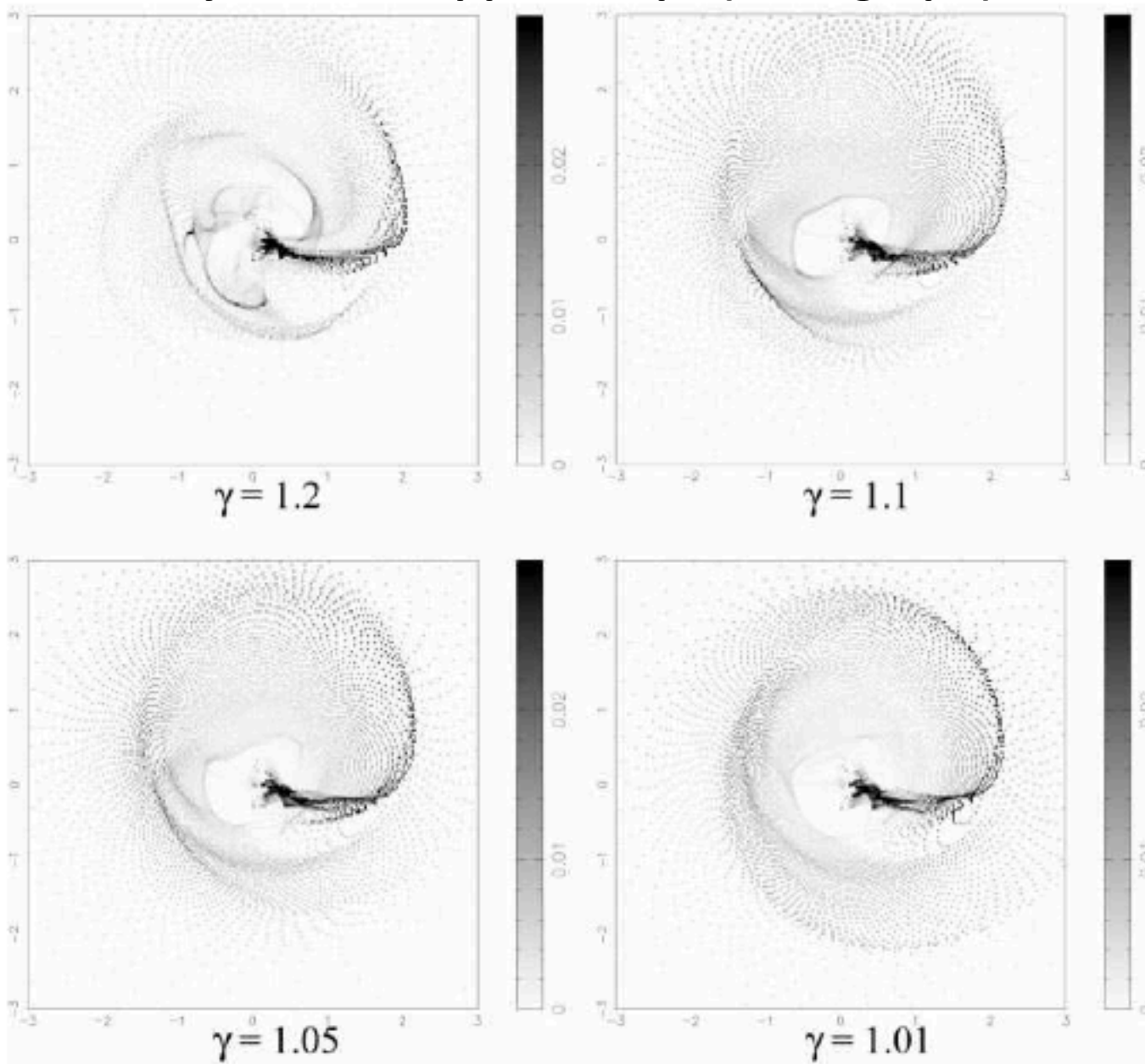


Figure 11. Doppler maps (hodograph) of 3D calculations in the orbital plane after five periods of revolution. Density profiles in velocity coordinates (V_x, V_y) are shown.

M. de Val-Borro, M. Karovska, and D. Sasselov 2009 (ApJ, 700,1148)

Model: symbiotic binaries, 2D, 128x384+3amr, hydro, using flash2.5, No self-gravity

Free parameters: mass-loss rate, wind temperature depends on the distance from the mass losing star and its companion, orbital separation.

Results: For typical AGB parameters the flow pattern is similar to a **Roche lobe overflow** with accretion rates of 10% of the mass loss from the primary. **Stable Keplerian thin disks**, exponential density profiles, $M \sim 10^{-4} M_{\text{sun}}$. Tidal streams and disks form and show a dependence with AGB mass loss. The evolution of **the binary system**, and its independent components, is **affected by mass transfer** through focused winds.

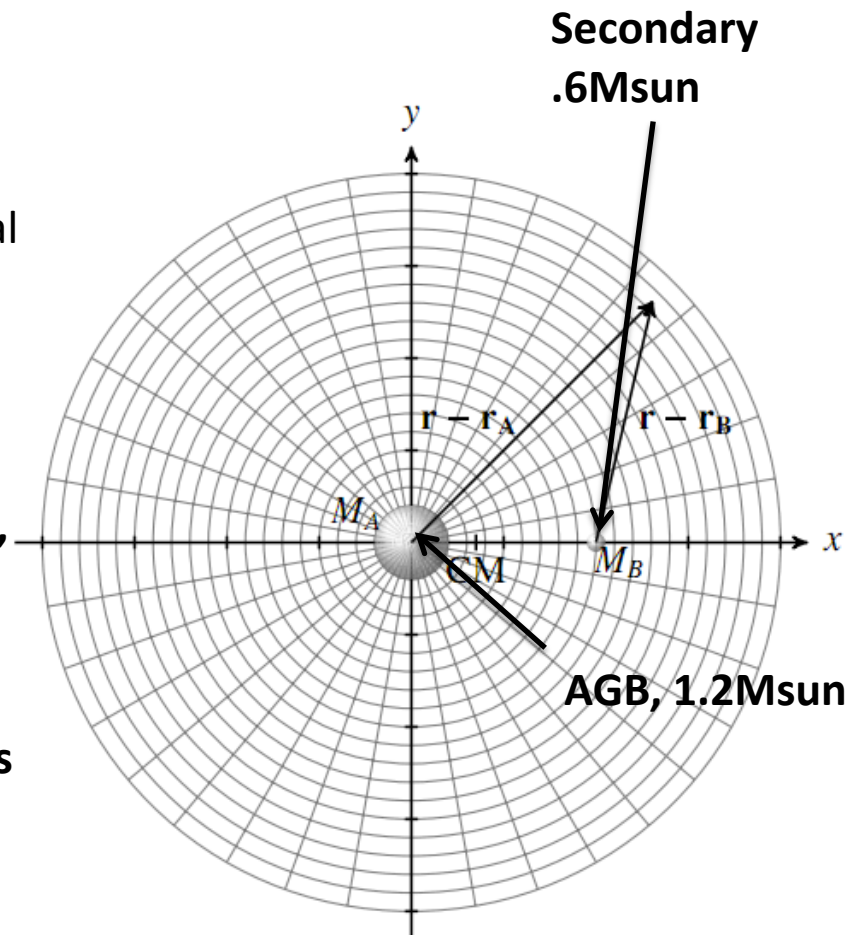


Figure 7. Schematic representation of the grid geometry in the polar coordinates. The physical quantities are defined in the center of the cells. The system is centered on the primary and rotating in clockwise direction.

Orbital
period

